Synthesis, structure and adsorption properties of a three-dimensional 3-fold interpenetrated Cd(II) coordination network with the rare tfz topology

ARTICLE *in* POLYHEDRON · APRIL 2015

Impact Factor: 2.01 · DOI: 10.1016/j.poly.2015.04.027

6 AUTHORS, INCLUDING:

Kedar Bahadur Thapa

Chung Yuan Christian University

6 PUBLICATIONS **1** CITATION

Polyhedron 96 (2015) 1–5

Contents lists available at ScienceDirect

Polyhedron

journal homepage: www.elsevier.com/locate/poly

Synthesis, structure and adsorption properties of a three-dimensional 3-fold interpenetrated Cd(II) coordination network with the rare **tfz** topology

Pei-Chi Cheng [a], Yang-Chih Lo [a], Wayne Hsu [a], Kedar Bahadur Thapa [a], Shih-Miao Liou [b,*], Jhy-Der Chen [a,*]

[a] Department of Chemistry, Chung Yuan Christian University, Chung-Li, Taiwan, ROC
[b] Center for General Education, Hsin Sheng Junior College of Medical Care and Management, Longtan, Taiwan, ROC

ARTICLE INFO

Article history:
Received 27 February 2015
Accepted 23 April 2015
Available online 1 May 2015

Keyword:
Coordination polymer

ABSTRACT

A three-dimensional (3D) coordination network $\{[Cd_3(BTC)_2(\mathbf{L})_3(H_2O)_3]\cdot 3H_2O\}_\infty$ [**L** = *N*,*N*′-di(4-pyridyl)adipoamide; H_3BTC = 1,3,5-benzenetricarboxylic acid], **1**, has been synthesized by the hydrothermal reaction and characterized by the single crystal X-ray crystallography. Structural analysis reveals that the BTC^{3-} ligands adopt the μ_3-bonding mode and coordinate to the Cd(II) ions to establish the triangular Cd(II) units, which are linked by the **L** ligands to form a 3-fold interpenetrated coordination network with the rare **tfz** topology. Gas adsorption experiments of the desolvated product of **1** show that the H_2 capture is preferable to N_2 and CO_2.

1. Introduction

Recently, the attentiveness of researchers towards the special characteristics of coordination polymers, i.e. catalysis, magnetism, luminescence and gas adsorption, in addition to their fascinating architectures and topologies, has been concentrated to an increasing extent [1,2]. It is widely known that the open structures having high porosities play vital role in determining the efficiency for gas adsorption. However, "nature abhors a vacuum", entanglement in a crystal may happen to maximize its packing efficiency [3]. Interpenetrating network is a significant subclass of entangled system, in which the voids associated with one network are occupied by one or more independent networks and they can be isolated only by breaking all the internal connections [2(d)]. The pore sizes of such coordination networks can be controlled to achieve selectivity in spite of the fact that interpenetration has been regarded as a drawback to porosity [2(e)]. Consequently, the design and synthesis of interpenetrating frameworks that show excellent selectivity in gas adsorption is a challenge in the crystal engineering of coordination polymers.

The dicarboxylate has been widely used as the auxiliary ligand for the construction of new coordination polymers [4]. We have reported several Cd(II) coordination polymers based on *N*,*N*′-di(4-pyridyl)adipoamide (**L**) and dicarboxylate ligands [5]. In this regard, a typical example is the 2-fold interpenetrated coordination network $[Cd(bpdc)(\mathbf{L})]_n$ [H_2bpdc = 4,4′-biphenyldicarboxylic acid] that adopts the **pcu** topology and revealed that the CO_2 capture is preferable to N_2 in the gas sorption experiments. This result signifies that the amide group of **L** and the entanglement of the coordination network may influence the adsorption of the light gases [5(b)]. Such supportive information encourages us to investigate the role of entanglement of coordination network containing tricarboxylate ligand and **L** in the gas adsorption. Herein, we report the synthesis, structure and adsorption properties of a three-dimensional 3-fold interpenetrated coordination network $\{[Cd_3(BTC)_2(\mathbf{L})_3(H_2O)_3]\cdot 3H_2O\}_\infty$ [H_3BTC = 1,3,5-benzenetricarboxylic acid], **1**, which shows that H_2 capture is preferable to N_2 and CO_2 in the gas adsorption. The C_3-symmetric tricarboxylate BTC^{3-} ligand plays an important structure-directing role in determining the **tfz** topology of **1**.

2. Experimental

2.1. General procedures

IR spectra (KBr disk) were obtained from a JASCO FT/IR-460 plus spectrometer. Elemental analyses were obtained from PE 2400 series II CHNS/O analyzer. Thermal gravimetric analyses (TGA) measurements were carried on SII Nano Technology Inc. TG/DTA 6200 over the temperature range of 30–900 °C at a heating rate of 10 °C min^{-1} under air. Powder X-ray diffraction instrument were carried out on Bruker D2 PHASER diffractometer with Cu Kα (λ_α = 1.54 Å) radiation.

* Corresponding authors. Tel.: +886 3 2653351; fax: +886 3 2653399.
E-mail addresses: lsm0301@hsc.edu.tw (S.-M. Liou), jdchen@cycu.edu.tw (J.-D. Chen).

http://dx.doi.org/10.1016/j.poly.2015.04.027
0277-5387/

2.2. Materials

The reagents $Cd(CH_3COO)_2{\cdot}2H_2O$ and H_3BTC (1,3,5-benzenetricarboxylic acid) were purchased from Aldrich Chemical Co. The ligands *N,N′*-di(4-pyridyl)adipoamide was prepared according to a published procedure [6].

2.3. Preparation

A mixture containing $Cd(CH_3COO)_2{\cdot}2H_2O$ (0.034 g, 0.15 mmol), 1,3,5-H_3BTC (0.021 g, 0.10 mmol), **L** (0.0447 g, 0.15 mmol) and H_2O (10 mL) was placed in a 23 mL Teflon lined stainless container. The container was then sealed and heated at 120 °C for 48 h under autogeneous pressure and then cooled down slowly to room temperature. Colorless block crystals were collected, washed by ether and then dried under vacuum. Yield: 0.079 g (90%, based on Cd). *Anal.* Calc. for $C_{22}H_{24}CdN_4O_8$ (MW = 584.85): C, 45.18; H, 4.14; N, 9.58. Found: C, 44.39; H, 4.33; N, 9.24%. IR (cm^{-1}): 3135(br), 1701(s), 1621(m), 1596(s), 1558(s), 1509(s), 1444(m), 1369(s), 1295(w), 842(w), 733(m).

2.4. X-ray crystallography

The diffraction data of complexes **1** was collected at 22 °C on a Bruker AXS SMART APEX II CCD diffractometer equipped with a graphite–monochromated Mo Kα (λ_α = 0.71073 Å) radiation [7]. Data reduction was carried out by use of well-established computational procedures [8]. The structure factors were obtained after Lorentz and polarization correction. An empirical absorption correction based on a series of "multi-scan" was applied to the data. The position of the heavier Cd atom was located by the Patterson method. The remaining atoms were found in a series of alternating difference Fourier maps and least-square refinements, whereas the hydrogen atoms were added by using the HADD command in SHELXTL 5.10. Basic information pertaining to crystal parameters and structural refinement is summarized in Table 1. Selected bond distances and angles are listed in Table 2.

Table 1
Crystal data for complex **1**.

Compound	**1**
Formula	$C_{22}H_{24}CdN_4O_8$
Formula weight	584.85
Crystal system	trigonal
Space group	*R*-3*c*
a (Å)	18.7100(2)
b (Å)	18.7100(2)
c (Å)	40.4095(5)
α (°)	90
β (°)	90
γ (°)	120
V (Å^3)	12250.7(2)
Z	18
D_{calc} (Mg/m^3)	1.427
F(000)	5328
μ (Mo Kα) (mm^{-1})	0.850
Range(2θ) for data collection (°)	4.36 ⩽ 2θ ⩽ 56.60
Independent reflections (R_{int})	3383 (0.0371)
Data/restraints/parameters	3383/0/177
Quality-of-fit indicator [c]	1.050
Final *R* indices[$I > 2\sigma(I)$] [a,b]	R_1 = 0.0316, wR_2 = 0.0908
R indices (all data)	R_1 = 0.0445, wR_2 = 0.0991

[a] $R_1 = \sum||F_o| - |F_c||/\sum|F_o|$.
[b] $wR_2 = [\sum w(F_o^2 - F_c^2)^2/\sum w(F_o^2)^2]^{1/2}$. $w = 1/[\sigma^2(F_o^2) + (ap)^2 + (bp)]$, $p = [\max(F_o^2$ or 0) + $2(F_c^2)]/3$. a = 0.0580, b = 22.6967, **1**.
[c] Quality-of-fit = $[\sum w(|F_o^2| - |F_c^2|)^2/(N_{observed} - N_{parameters})]^{1/2}$.

Table 2
Selected bond distances (Å) and angles (°) for **1**.

Bond distances			
Cd–N(1)	2.332(2)	Cd–N(1A)	2.332(2)
Cd–O(2)	2.492(2)	Cd–O(2A)	2.492(2)
Cd–O(3)	2.323(2)	Cd–O(3A)	2.323(2)
Cd–O(4)	2.380(4)		
Bond angles			
N(1)–Cd–N(1A)	176.91(13)	N(1)–Cd–O(2)	89.66(7)
N(1)–Cd–O(2A)	88.11(8)	N(1)–Cd–O(4)	91.55(6)
N(1A)–Cd–O(2)	88.11(8)	N(1A)–Cd–O(2A)	89.67(7)
N(1A)–Cd–O(4)	91.55(6)	O(2A)–Cd–O(2)	87.94(8)
O(3)–Cd–N(1)	92.34(8)	O(3)–Cd–N(1A)	88.11(8)
O(3)–Cd–O(2)	54.45(6)	O(3)–Cd–O(2A)	142.37(7)
O(3)–Cd–O(4)	81.59(5)	O(3A)–Cd–N(1)	88.11(8)
O(3A)–Cd–N(1A)	92.34(8)	O(3A)–Cd–O(2)	142.37(7)
O(3A)–Cd–O(2A)	54.45(6)	O(3A)–Cd–O(3)	163.18(10)
O(3A)–Cd–O(4)	81.59(5)	O(4)–Cd–O(2)	136.03(4)
O(4)–Cd–O(2A)	136.03(4)		

Symmetry transformations used to generate equivalent atoms: (A) $-x + 4/3, -x + y + 2/3, -z + 1/6$.

2.5. Gas adsorption measurements

The adsorption isotherms for N_2, H_2, and CO_2 were carried out on a Micrometrics ASAP 2020 Series analyzer by using gases of the highest quality at 77 and 293 K in a liquid nitrogen bath, and an ice-water bath, respectively. Before the measurement, the sample was degassed (10^{-3} torr) at 423 K overnight to remove the cocrystallized water molecules.

3. Results and discussion

3.1. Structure of *1*

Fig. 1(a) depicts a drawing showing the coordination environment about the Cd(II) ion, which is coordinated by two pyridyl nitrogen atoms of two **L** ligands [Cd–N = 2.332(2) Å], four carboxylate oxygen atoms of two 1,3,5-BTC ligands [Cd–O = 2.323(2)–2.492(2) Å] and one coordinated water molecule [Cd–O = 2.380(4) Å], resulting in a distorted pentagonal bipyramidal geometry. Four oxygen atoms of two 1,3,5-BTC ligands and one oxygen atoms of water molecule are located in the equatorial plane with the Cd(II) center deviating from the plane by 0.11 Å, while two pyridyl nitrogen atoms of the **L** ligands occupy the axial positions. The Cd(II) ions are linked by the $\mu_3,\eta^1,\eta^1,\eta^1,\eta^1,\eta^1,\eta^1$-1,3,5-$BTC^{3-}$ ligands to form layered substructures (Cd–Cd = 9.73 Å) that are pillared by the long **L** ligands (20.44 Å) to form a 3D framework, Fig. 1(b), (c). The **L** ligands adopt the GAG *trans* conformation [5,6]. Topological analysis reveals that complex **1** forms a rare binodal 3,4-connected 3-fold interpenetrated coordination network (Class Ia) with the $\{6^3\}_2\{64{\cdot}8{\cdot}10\}_3$-**tfz** topology, Fig. 1(d), determined using TOPOS [9]. Despite the occurrence of 3-fold interpenetration, there remains a considerable void space occupied by water molecules. The solvent accessible volume calculated without including lattice water by PLATON [10] analysis is 3213.8 Å^3 which is 26.2% of the unit cell volume.

The underlying **tfz** net is observed in 9 crystals (interpenetrated in 5) and can be found in TTD database of TOPOS. Although four examples of a triply interpenetrated **tfz** net have been reported for metal–organic compounds, there are in fact only two different compounds presently known, which are $[Cu_3(BTC)_2(L^1)_3]$ [L^1 = *N,N′*-bis(4-pyridylformamide)-1,4-benzene] [11(a),(c)] and $[Ni_3(BTB)_2(EG)_3(bipy)_3]{\cdot}$(toluene) (BTB = 1,3,5-benzenetrisbenzoate; EG = ethylene glycol; bipy = 4,4′-bipyridyl) [11(b)]. The other two compounds are the same as $[Cu_3(BTC)_2(L^1)_3]$ with different co-crystallized water molecules. Since the neutral bipy ligand of $[Ni_3(BTB)_2(EG)_3(bipy)_3]{\cdot}$(toluene), L^1 ligand of $[Cu_3(BTC)_2(L^1)_3]$ and

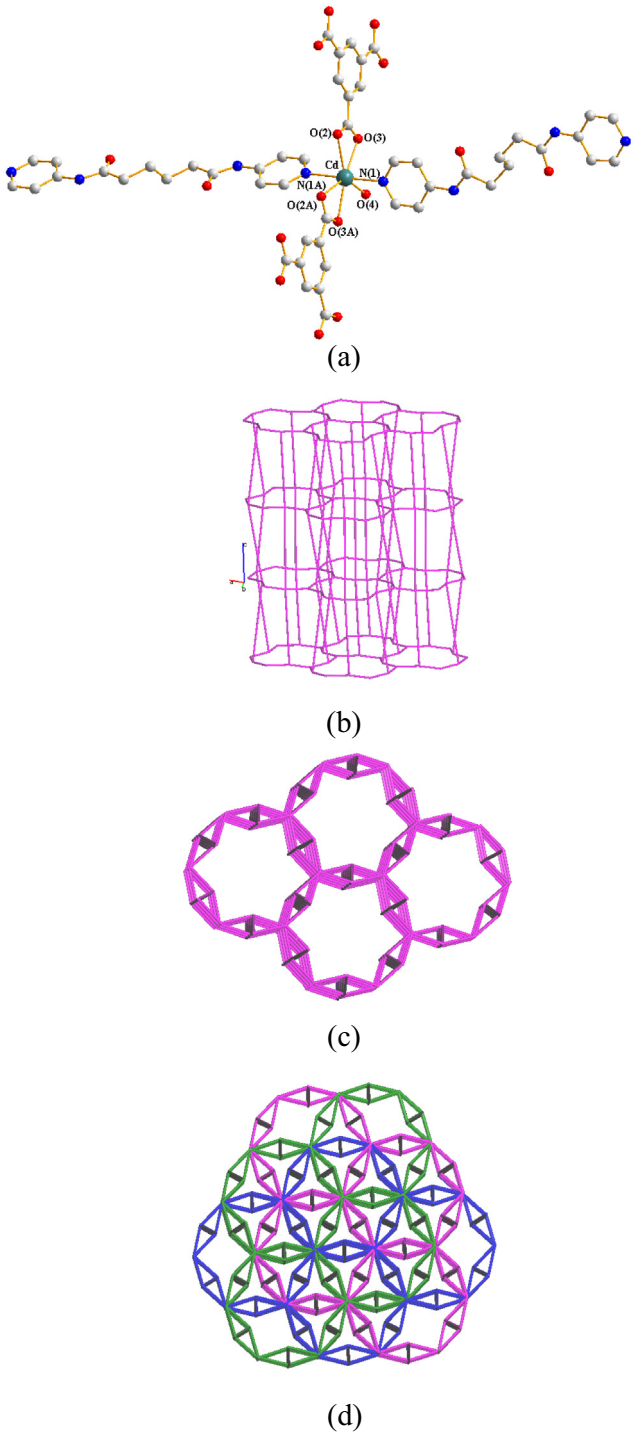

Fig. 1. (a) A drawing showing the coordination environment about the Cd(II) ion. (b) A view of the 3D coordination network with the **tfz** topology, looking down the *b* axis. (c) Another view looking down the *c* axis. (d) A drawing showing the 3-fold interpenetrated coordination network.

L ligand of **1** are rigid, semi-rigid and flexible ligands, respectively, it can be concluded that the C_3-symmetric tricarboxylate ligands play the most important structure-directing role in forming the 3-fold interpenetrated coordination network with the **tfz** topology.

3.2. Thermal and luminescent properties

The thermal stability of complex **1** was examined by thermogravimetric analysis (TGA) in N_2 atmosphere from 30 to 900 °C.

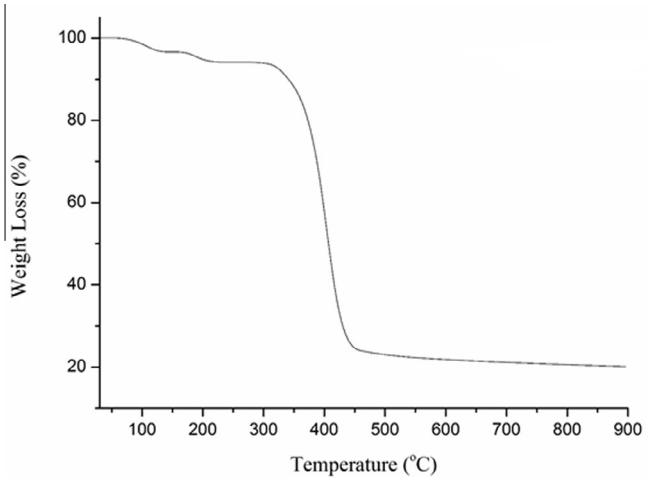

Fig. 2. TGA curve of **1**.

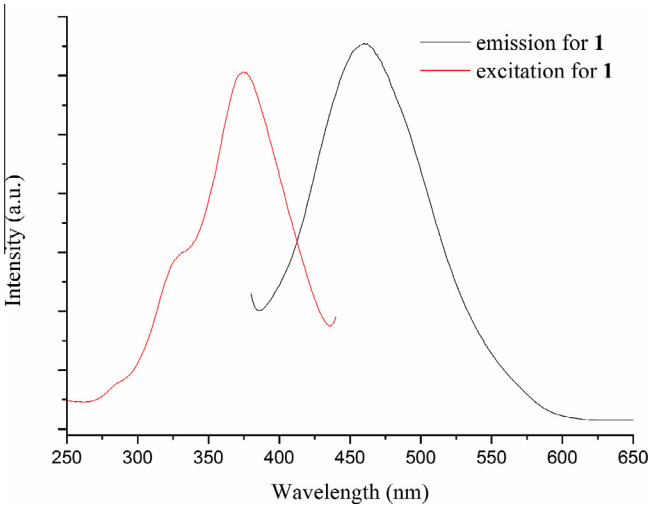

Fig. 3. Excitation and emission spectra of **1**.

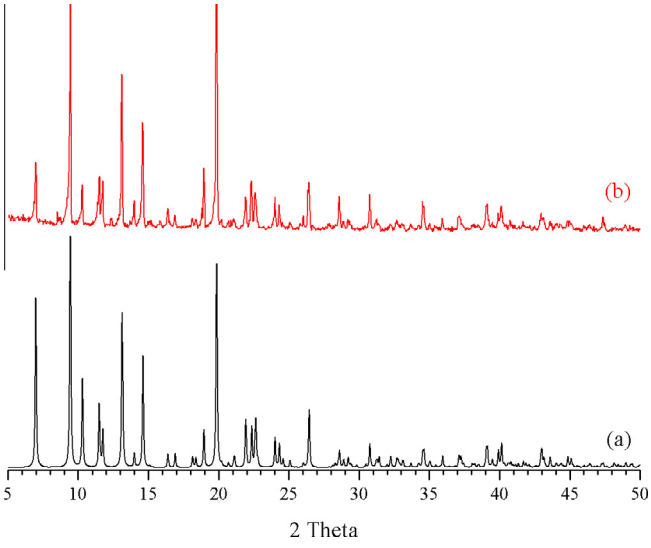

Fig. 4. (a) Simulated and (b) experimental PXRD patterns for **1**.

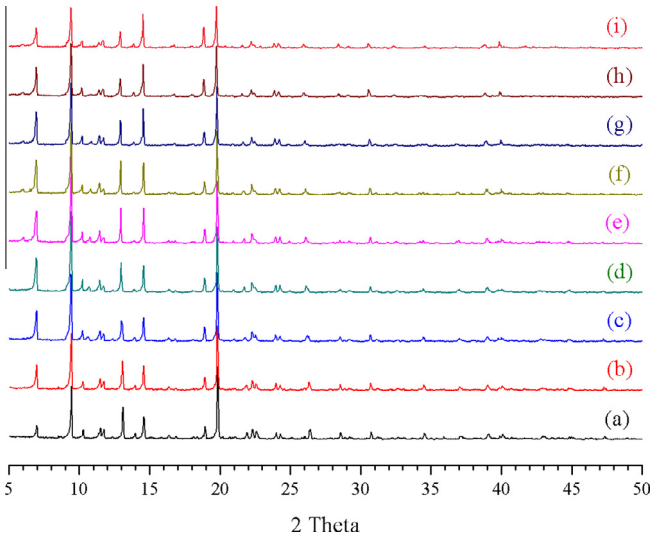

Fig. 5. The PXRD patterns of **1** at (a) 30 °C, (b) 60 °C, (c) 90 °C, (d) 120 °C, (e) 150 °C, (f) 180 °C, (g) 210 °C, (h) 240 °C and (i) 270 °C.

As shown in Fig. 2, the first weight loss of 3.3% occurs between 90 and 125 °C, corresponding to the removal of the cocrystallized water molecules (calcd 3.1%), whereas the second weight loss of 2.9% in 165–210 °C is due to the bonded water molecules (calcd 3.1%). In the range of 305–460 °C, the third weight loss of 72.3% can be ascribed to the decomposition of the **L** and BTC^{3-} ligands (calcd 74.6%).

The free **L** and 1,3,5-H_3BTC ligands show emissions at 405 and 325 nm, upon excitation at 364 and 301 nm, respectively, which may be tentatively ascribed to the intraligand (IL) $n \rightarrow \pi^*$ or $\pi \rightarrow \pi^*$ transitions [5(b),12]. Complex **1** shows emission at 460 nm upon excitation at 374 nm, Fig. 3. We attribute the emission of **1** to the intraligand and/or the ligand-to-ligand charge transfer (LLCT). The possibility of ligand-to-metal charge transfer (LMCT) or metal-to-ligand charge transfer (MLCT) can be excluded due to the difficulty to oxidize or reduce the d^{10} Cd(II) ions [13]. The red shift of the emission of **1** with respect to the free organic ligands can be ascribed to the different ligand conformations and coordination modes resulting from the coordination of the ligands to the Cd(II) ions.

3.3. Gas sorption

Although the structure of **1** is triply interpenetrated, there is a large solvent accessible volume of 26.2% per unit cell. We thus carried out the gas sorption experiments for the desolvated product of **1**, **1′**, to investigate its pore structure and gas storage capability. Fig. 4 shows that the powder pattern of **1** agrees quite well with the simulated one from single-crystal X-ray data, which indicates the bulk purity of **1**. Fig. 5 shows the variable temperature powder patterns for **1**, and accordingly, **1** was stable upon removal of solvents. The sample for gas sorption investigation was then heated up to 150 °C (from TGA) to remove the solvent molecules before the measurement.

The N_2, H_2 and CO_2 adsorption isotherms of **1′** are shown in Fig. 6. The results indicate that the degree of N_2 adsorption (77 K) is only minimal, but higher amounts of H_2 (77 K) and CO_2 (273 K) are adsorbed and the H_2 capture is preferable to N_2 and CO_2 in the gas adsorption. The Langmuir and BET surface areas estimated from the N_2 sorption isotherm are 20.3 and 7.5 $m^2\,g^{-1}$, respectively. The maximum CO_2 adsorptions amount at 1 atm are 0.207 and 0.122 mmol/g at 273 and 298 K, respectively, and the H_2 sorption

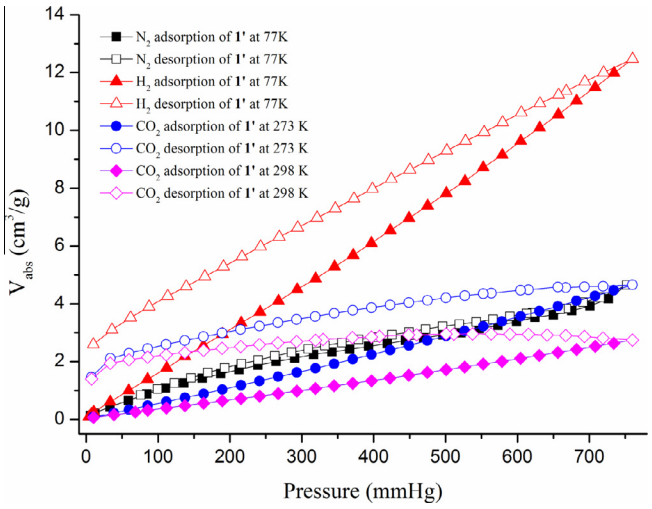

Fig. 6. Adsorption isotherms of of **1′**.

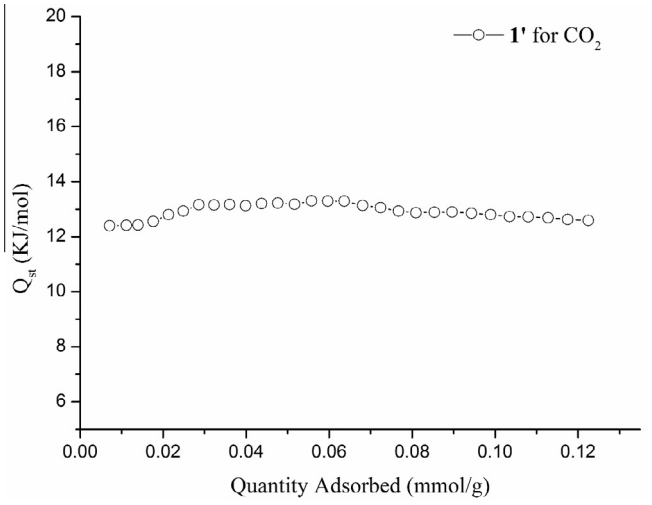

Fig. 7. Isosteric heat of adsorption of **1′** at different CO_2 uptake amounts.

measurement at 77 K shows a 0.111 wt% hydrogen uptake at 1 atm. In addition, hysteresis between H_2 adsorption and desorption isotherms demonstrates that H_2 adsorption is irreversible. This may be due to the confinement effect of H_2 in the 3-fold interpenetrated coordination network. The Clausius–Clapeyron equation implemented in the software of the Micrometrics ASAP 2020 sorptometer was employed to calculate the isosteric heats (Q_{st}) of CO_2 adsorption at 273 and 298 K. The Q_{st} against loading amount is illustrated in Fig. 7, which exhibits a highest value of 13.30 kJ/mol at 0.056 mmol/g CO_2 uptake and decreases slowly with increasing CO_2. The small Q_{st} values indicate physical adsorption for CO_2 [14].

The present result suggests that for the triply interpenetrated coordination network **1**, the H_2 sorption is more accessible than N_2 and CO_2 sorptions. This consequence is in marked contrast to that of the 2-fold interpenetrated coordination network $[Cd(bpdc)(\mathbf{L})]_n$ showing that the CO_2 capture is preferable to N_2 [5(b)].

4. Conclusions

By the hydrothermal reaction of $Cd(CH_3COO)_2{\cdot}2H_2O$, H_3BTC and **L**, we have prepared the complex $\{[Cd_3(BTC)_2(\mathbf{L})_3(H_2O)_3]{\cdot}3H_2O\}_\infty$, **1**, which forms a 3-fold interpenetrated 3D coordination network

with the rare **tfz** topology. A comparison of **1** with the other similar complexes indicates that the C_3-symmetric tricarboxylate ligands play the most important structure-directing role in forming the 3-fold interpenetrated coordination network with the **tfz** topology. The adsorption investigations of the desolvated product of **1** reveal that the H_2 capture is preferable to N_2 and CO_2. The entanglement of coordination networks may play some important roles in the selectivity of light gases in the sorption experiments.

Acknowledgment

We are grateful to the Ministry of Science and Technology of the Republic of China for support.

Appendix A. Supplementary data

CCDC 1041483 contains the supplementary crystallographic data for compound **1**. These data can be obtained free of charge via http://www.ccdc.cam.ac.uk/conts/retrieving.html, or from the Cambridge Crystallographic Data Centre, 12 Union Road, Cambridge CB2 1EZ, UK. Fax: +44 1223 336 033; or e-mail: deposit@ccdc.cam.ac.uk.

References

[1] (a) Y. Yamauchi, M. Yoshizawa, M. Fujita, J. Am. Chem. Soc. 130 (2008) 5932;
(b) H.-C. Zhou, J.R. Long, O.M. Yaghi, Chem. Rev. 112 (2012) 673;
(c) Z. Yin, Q.-X. Wang, M.-H. Zeng, J. Am. Chem. Soc. 134 (2012) 4857.
[2] (a) I.A. Baburin, V.A. Blatov, L. Carlucci, G. Ciani, D.M. Proserpio, CrystEngComm 10 (2008) 1822;
(b) V.A. Blatov, L. Carlucci, G. Ciani, D.M. Proserpio, CrystEngComm 6 (2004) 377;
(c) I.A. Baburin, V.A. Blatov, L. Carlucci, G. Ciani, D.M. Proserpio, J. Solid State Chem. 178 (2005) 2452;
(d) L. Carlucci, G. Ciani, D.M. Proserpio, Coord. Chem. Rev. 246 (2003) 247;
(e) O.M. Yaghi, Nat. Mater. 6 (2007) 92.
[3] S.R. Batten, S.M. Neville, D.R. Turner, Coordination Polymers: Design, Analysis and Application, Royal Society of Chemistry, Cambridge, 2009.
[4] (a) M. Du, X.-J. Jiang, X.-J. Zhao, Chem. Commun. (2005) 5521;
(b) M. Du, Z.-H. Zhang, X.-G. Wang, L.-F. Tang, X.-J. Zhao, CrystEngComm 10 (2008) 1855;
(c) M. Du, X.-J. Jiang, X.-J. Zhao, Inorg. Chem. 46 (2007) 3984;
(d) J. Yang, J.-F. Ma, Y.-Y. Liu, J.-C. Ma, S.R. Batten, Cryst. Growth Des. 9 (2009) 1894.
[5] (a) J.-J. Cheng, Y.-T. Chang, C.-J. Wu, Y.-F. Hsu, C.-H. Lin, D.M. Proserpio, J.-D. Chen, CrystEngComm 14 (2012) 537;
(b) M.-J. Sie, Y.-J. Chang, P.-W. Cheng, P.-T. Kuo, C.-W. Yeh, C.-F. Cheng, J.-D. Chen, J.-C. Wang, CrystEngComm 14 (2012) 5505.
[6] Y.-F. Hsu, H.-L. Hu, C.-J. Wu, C.-W. Yeh, D.M. Proserpio, J.-D. Chen, CrystEngComm 11 (2009) 168.
[7] Bruker AXS, APEX2, V2008.6; SADABS V2008/1; SAINT V7.60A; SHELXTL V6.14; Bruker AXS Inc., Madison, Wisconsin, USA, 2008.
[8] G.M. Sheldrick, Acta Crystallogr., Sect. A 64 (2008) 112.
[9] V.A. Blatov, A.P. Shevchenko, D.M. Proserpio, Cryst. Growth Des. 14 (2014) 3576. See also: http://www.topos.samsu.ru/.
[10] A.L. Spek, J. Appl. Crystallogr. 36 (2003) 7.
[11] (a) F. Luo, J.-M. Zheng, S.R. Batten, Chem. Comm. (2007) 3744;
(b) R. Heck, J. Basca, J.E. Warren, M.J. Rosseinsky, D. Bradshaw, CrystEngComm 10 (2008) 1687;
(c) X. Wang, H. Lin, B. Mu, A. Tian, G. Liu, Dalton Trans. 39 (2010) 187.
[12] P.-C. Cheng, M.-H. Wu, M.-Y. Xie, W.-J. Huang, H.-Y. He, T.-T. Wu, Y.-C. Lo, D.M. Proserpio, J.-D. Chen, CrystEngComm 15 (2013) 10346.
[13] (a) L.-F. Ma, L.-Y. Wang, J.-L. Hu, Y.-Y. Wang, G.-P. Yang, Cryst. Growth Des. 9 (2009) 5334;
(b) D. Sun, Z.-H. Yan, V.A. Blatov, L. Wang, D.-F. Sun, Cryst. Growth Des. 13 (2013) 1277.
[14] (a) Q.M. Wang, D. Shen, M. Bülow, M.L. Lau, S. Deng, F.R. Fitch, N.O. Lemcoff, L. Semanscin, Microporous Mesoporous Mater. 55 (2002) 217;
(b) J.A. Dunne, M. Rao, S. Sircar, R.J. Gorte, A.L. Myers, Langmuir 12 (1996) 5896.